Deep Radiomic Analysis of MRI Related to Alzheimer's Disease

AHMAD CHADDAD[1,2], **CHRISTIAN DESROSIERS**[3], **AND TAMIM NIAZI**[2]

[1]Department of Automated Manufacturing Engineering, Ecole de Technologie Supérieure, University of Quebec, Montreal, QC H3C 1K3, Canada
[2]Department of Radiation Oncology, McGill University, Montreal, QC H3A 0G4, Canada
[3]Department of Software and IT Engineering, Ecole de Technologie Supérieure, University of Quebec, Montreal, QC H3C 1K3, Canada

Corresponding author: Ahmad Chaddad (achaddad@livia.etsmtl.ca; ahmad.chaddad@mail.mcgill.ca)

ABSTRACT Alzheimer's disease (AD) is the most common form of dementia, causing progressive impairment of memory and cognitive functions. Radiomic features obtained from brain MRI have shown a great potential as non-invasive biomarkers for this disease; however, their usefulness has not yet been explored for individual brain regions. In this paper, we hypothesize that distinct regions are affected differently by AD and, thus, that shape or texture changes occurring in separate regions can be expressed by different radiomic features. Moreover, to improve the classification of AD and healthy control (HC) subjects, we propose novel features based on the entropy of the convolution neural network (CNN) feature maps. The proposed approach is evaluated comprehensively using the Open Access Series of Imaging Studies database. Our experiments assess the significance of 45 different radiomic features from individual subcortical regions, via the Wilcoxon test. We also use the random forest classifier to identify the subcortical regions that best differentiate AD patients from HC subjects. Our analysis identified the features derived from several subcortical regions that show significant differences between AD and HC (corrected $p < 0.01$). Specifically, we found correlation and volume features from the hippocampus (AUC $= 81.19\% - 84.09\%$) and amygdala (AUC $= 79.70\% - 80.27\%$) regions to have the greatest discriminative power. Furthermore, the proposed entropy features derived from CNN layers yielded the highest classification AUC of 92.58%, compared to 84.45% for the combined radiomic features of all subcortical. These results suggest that the proposed CNN entropy features could be used as an effective biomarker for AD.

INDEX TERMS Alzheimer's, radiomics, classification.

I. INTRODUCTION

Alzheimer's disease (AD) is a progressive neurodegenerative disorder which represents the most common cause of dementia in the elderly [1]. Its symptoms consist of memory loss, confusion in time and place, lack of communication with others and failure to recognize close ones [2]. While AD patients constitute 2% of the population at the age of 65 years, this number increases to 30% at the age of 85 years [3]. Moreover, the total number of AD sufferers is expected to double in the next 20 years, with around 1/85 people affected by 2050 [4]. Many efforts have been made to better understand AD and find an effective treatment, however there currently exists no treatment to cure or slow the progression of this disorder [5]. As Alzheimer progresses, brain cells die and connections among these cells are lost, which produces cognitive symptoms. This anatomo-pathology can be visualized non-invasively via MRI imaging, and described quantitatively by

radiomic analysis. In general, AD is characterized by cortical atrophy in regions like the hippocampus, and by the enlargement of extra cerebral spaces. Figure 1 illustrates differences between AD and healthy control (HC) brains using 3D brain MRI.

Non-invasive imaging features are a very promising technique to characterize the cortex and subcortical regions of AD patients. A variety of studies have been proposed to characterize and predict AD [5], [7]–[13] with the most important biomarkers detected as brain volume and thickness. Villain *et al.* [14] showed that the hippocampus of AD patients is a third smaller than in healthy subjects. A study of anatomical region differences in AD patients revealed that the mesial temporal region is the most effective region in the brain to identify patients with mild cognitive impairment (MCI) [15]. A feature-based morphometry approach, which considered the scale-invariant features transform (SIFT)
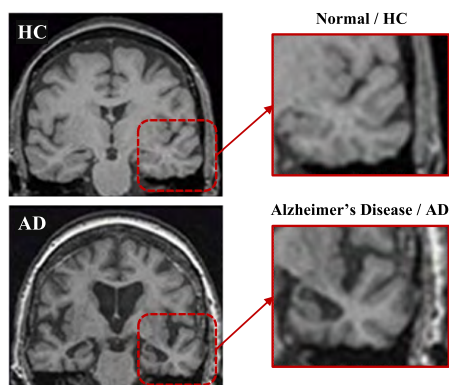
FIGURE 1. MRI slice of 3D brain illustrating the differences between a healthy control subject (HC, first row) and Alzheimer's disease (AD, second row). A zoom view of the images shows an atrophy of the cortical surface (in the red cadre) involving the hippocampus area that related to the short-term memory formation in AD patients.

model, was also able to identify several structural differences between AD and healthy control (HC) subjects [16]. Employing other invariant features, such as Gray-level Invariant features (GLIF), confirmed differences between AD and HC using multicenter datasets [17]. It was found that, with increasing age, HC subjects could transform to AD [18] or dementia [19] through changes occurring in white matter regions [20]. Such changes, including cerebral thinning, could lead to cognitive decline [21] as well as to poor episodic memory, late-life depression and MCI [22].

In the last decade, radiomic approaches have been widely considered for medical image analysis [6], [23], [24]. Such approaches extract texture or shape features from medical images like MRI, which are correlated to patient/disease characteristics. Several types of texture features, including SIFT [25], GLCM [26] and wavelets filters [27], have shown their relevance in the detection and quantification of various diseases. For example, textural features based on co-occurrence matrix and run-length matrix were shown to differentiate patients with AD from those with dementia Lewy bodies [28]. Similarly, 3D texture features extracted from the hippocampus and entorhinal cortex were significantly different in AD patients compared to healthy controls [29]. Abnormalities of hippocampal texture in MCI patients has also been shown to be prognostic of early cognitive decline [30].

A recent study showed that constructing individual hierarchical networks of six 3D texture features from brain images indicates differences between tissues in AD, MCI, and HC [31]. Another study considered the combination of volume, cortical thickness, and hippocampal shape/texture for the diagnosis of HC, MCI, and AD. It was shown that hippocampal texture was the most important feature for prediction, followed by hippocampal volume, ventricular volume, and parietal lobe thickness [32].

So far, most radiomic studies have focused on extracting features from whole brains or from target subcortical regions like the hippocampus. Since different brain regions can be affected by AD in a distinct manner, we hypothesize in this work that analyzing texture in individual subcortical regions can lead to a better classification of AD and HC subjects. This is based on the idea that the characteristics of separate brain regions can be best captured by different texture features. Moreover, although some researchers have proposed using deep learning techniques like convolution neural networks (CNNs) to classify AD or MCI patients [33], deep features have not yet been compared to traditional features in a single radiomic analysis.

This manuscript proposes a deep radiomic analysis of subcortical region features for the classification of AD and HC subjects. The two main contributions of this study are: 1) A comprehensive analysis of traditional radiomic features in individual subcortical regions labeled using an atlas. 2) A novel technique, based on the entropy of convolutional feature maps, to characterize local texture in a data-driven manner. Our experiments show that the proposed CNN entropy features lead to a higher classification accuracy.

The rest of this paper is structured as follows. Section 2 describes the population, image data and proposed radiomic features for classifying AD from HC subjects. Section 3 provides experimental setup and results. Section 4 discusses our finding. Finally, Section 5 concludes with a summary of our work's main contributions and results.

II. MATERIALS AND METHODS

We use radiomic features derived from brain MRI data to find associations between subcortical regions and AD. Employing the processing pipeline of Freesurfer [34], MRI volumes are first registered to an atlas and labeled into 25 key subcortical regions: left/right Cerebral-White-Matter, left/right Cerebellum-White Matter, left/right Thalamus-Proper, left/right Caudate, left/right Putamen, left/right Pallidum, left/right Hippocampus, left/right Amygdala, left/right Accumbens-area, left/right VentralDC, left/right Vessel, Optic-Chiasm, Brain-Stem, and Cerebrospinal Fluid (CSF). A total of 45 radiomic features derived from intensity histograms, gray level co-occurrence matrix (GLCM), neighborhood gray-tone difference matrix (NGTDM), and gray-level size zone matrix (GLSZM) are then computed in subcortical regions of each MRI scan.

A significance test was performed to identify features in each region exhibiting significant differences between AD and HC subjects. Radiomic features in different subcortical regions were then used as input to a random forest model for classifying AD and HC subjects. To improve classification, we also proposed novel radiomic features based on the entropy in convolution layers of a deep CNN [35]. Figure 2 shows a flowchart of the proposed approach. The following sections describe each step of our approach in greater detail.

A. PARTICIPANTS AND DATA ACQUISITION

The data used in this study were obtained from The Open Access Series of Imaging Studies (OASIS) database
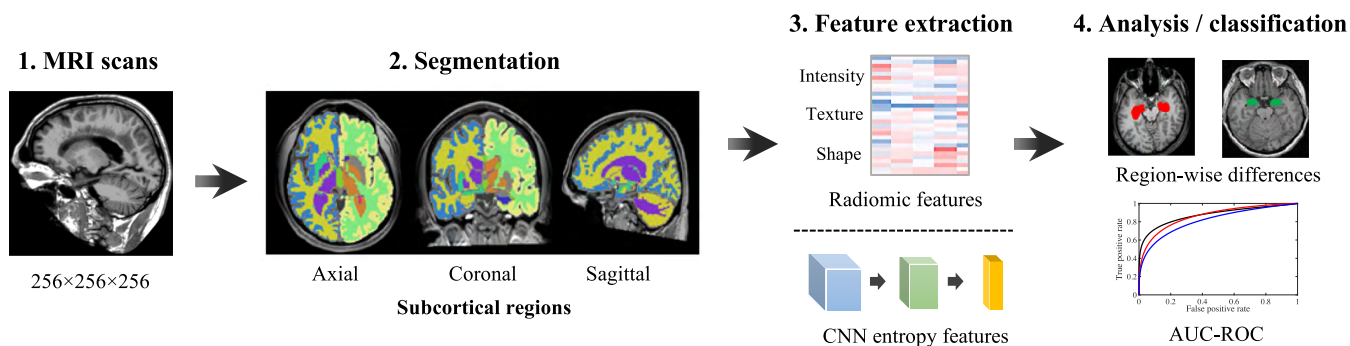
FIGURE 2. Processing pipeline of the proposed radiomic analysis. 1) T1 weighted MR images are acquired. 2) Subcortical brain regions are labeled using FreeSurfer. 3) Features are extracted from each region, quantifying intensity, shape and texture. 4) Features analysis and classification between AD and HC.

TABLE 1. Demographics and clinical information for AD and HC subjects.

Variable	HC (N=135)	AD (N=100)	*p* value
CDR	0	0.5-2	
Age, median (min-max)	71 (33-94)	77 (62-96)	*2.6×10^{-5}
Sex, male/female	38/97	41/59	**2.7×10^{-6}
MMSE score, median (min-max)	29 (25-30)	26(14-30)	*5.03×10^{-25}
Legends: *Wilcoxon rank test; ** Fisher exact test.			

(http://www.oasis-brains.org) [36]. This database is made available by the Washington University Alzheimer's Disease Research Center, Dr. Randy Buckner at the Howard Hughes Medical Institute (HHMI) at Harvard University, the Neuroinformatics Research Group (NRG) at Washington University School of Medicine, and the Biomedical Informatics Research Network (BIRN). The goal of OASIS is to offer MRI dataset of the brain freely available to the scientific community in order to facilitate future discoveries in basic and clinical neuroscience. For up-to-date information, see http://www.oasis-brains.org/.

The OASIS 1 database consists of 416 right-handed HC and patients with early-stage AD, with 3D T1-weighted magnetization prepared rapid gradient echo (MPRAGE) images acquired at 1.5 Tesla (i.e., specifications are repetition time (TR) = 9.7 ms, inversion time (TI) = 20 ms, flip angle = 10°, echo time (TE) = 4.0 ms). The MRI protocol was the same for all subjects with more details available in [36]. All data are anonymized with no protected health information included. Image acquired with a resolution of 1 mm³, for a total size of 256×256×256 voxels.

Our study included T1-weighted MRI data from the 135 available HC subjects with Clinical Dementia Rating (CDR) of 0, and from 100 AD patients (70 with CDR=0.5, 28 with CDR=1, and 2 with CDR=2). Subjects with unknown CDR score were excluded from this study. The demographic and clinical characteristics of AD and HC subjects in the database are reported in Table 1.

B. IMAGE PROCESSING

We use a preprocessed version of the OASIS database, which is publicly available for download.[1] T1 weighted MR images were processed using Freesurfer[2] [34], following the following six steps: 1) small-motion correction by averaging the available volumes of subjects, 2) (non-uniform) intensity normalization, 3) affine registration of volumes to the MNI305 atlas, 4) skull-stripping, 5) non-linear registration and further normalization using the Gaussian Classifier Atlas (GCA), and 6) brain parcellation and subcortical region labeling using the GCA. The final outputs of this pipeline tool are the skull-stripped, intensity normalized brain volumes in the subject space (i.e., the *brain.mgz* file), and the sub-cortical labeling of these volumes into 41 hemisphere-distinct regions (i.e., the *aseg.mgz* file).

C. RADIOMIC FEATURES

We extracted various radiomic features characterizing the heterogeneity and shape of subcortical regions. Specifically, we extracted 3D GLCMs of image intensities uniformly resampled to 32 gray-levels, considering the combination of 13 angles and 4 offsets/displacements [37]. Each of the 52 resulting GLCM matrices were converted to a feature vector by applying 19 different quantifier functions: angular second moment, contrast, correlation, sum of squares variance, homogeneity, sum average, sum variance, sum entropy, entropy, difference variance, difference entropy, information correlation 1, information correlation 2, autocorrelation, dissimilarity, cluster shape, cluster prominence, maximum probability and inverse difference [38]. Finally, these 52 vectors were averaged into a single vector of 19 features.

Following a similar process, we also computed 5 features based on NGTDM (i.e., coarseness, contrast, busyness, complexity and texture strength [39]), as well as 11 features based on GLSZM (i.e., small zone size emphasis, large zone size

---

[1]http://ftp.nrg.wustl.edu
[2]http://surfer.nmr.mgh.harvard.edu/

emphasis, low gray-level zone emphasis, high gray-level zone emphasis, small zone / low gray emphasis, small zone / high gray emphasis, large zone / low gray emphasis, large zone / high gray emphasis, gray-level non-uniformity, zone size non-uniformity and zone size percentage [40]). Combining GLCM, NGTDM and GLSZM features, we obtained a total of 35 texture features measuring the heterogeneity of subcortical regions.

In addition to texture features, we also encoded the morphological characteristics of subcortical regions using 4 shape features: porosity, fraction dimension, surface-area and volume [41]. The volume and surface area of the hippocampus are known biomarkers for detecting AD [42]. Lastly, we summarized the distribution of voxel intensities in subcortical regions via 6 additional features: average, variance, skewness, kurtosis, energy and entropy. The 45 resulting features were considered in uni- and multi-variate analyses to identify the subcortical regions showing significant differences between AD and HC, and determine the most important features for classifying these two subject groups.

D. PROPOSED CNN ENTROPY FEATURES

As deep learning models have recently achieved state-of-the-art performance in different medical applications [43], we used the features learned by a convolution neural network (CNN) [44]–[46] to improve the classification of AD and HC subjects. Toward this goal, we considered the feature maps of convolutional layers as texture images, and measured the heterogeneity of this texture via entropy. As described in [35], we considered a 3D CNN architecture composed of 5 layers:

Input:	Image size = $256 \times 256 \times 256$ voxels
Layer-1:	Filter size = $2 \times 2 \times 2$; stride=2; filters=10; Max pooling; ReLU; output=10 feature maps of size $128 \times 128 \times 128$
Layer-2:	Filter size = $2 \times 2 \times 2$; stride=2; filters=10; Max pooling; ReLU; output=10 feature maps of size $64 \times 64 \times 64$
Layer-3:	Fully connected layer; output=vector size 128
Output:	AD class probability

The 21 feature maps produced by convolutional layers (i.e., 10 from Layer-1, 10 from Layer-2 and 1 from Layer-3) are considered as filtered images, from which are derived 21 entropy values. The entropy in each feature map is measured on the histogram of values constructed using 256 bins.

This approach is related to the Information Bottleneck theory [47], where information flow through a CNN is modeled as Markov chain and quantified via the mutual information between network filters. Here, we leverage the principle that, for a discriminatively trained filter set F, the entropy $H(Y|C, F)$ of CNN features Y conditioned on the class C and filter set F is a highly class-informative code, and that small sets of conditional entropy features can be used to improve

CNN classification. More details about this approach can be found in [35].

E. STATISTICAL ANALYSES

We applied the Wilcoxon non-parametric test to identify subcortical brain regions where the distribution of texture features is significantly different in AD and HC subjects. Since we perform multiple comparisons (i.e., 25 sub-cortical regions × 45 texture features = 1125 tests), we corrected obtained p values according to the Holm-Bonferroni method [48], and then considered corrected $p < 0.01$ as significance threshold.

For the multivariate analysis, the area under the receiver operating characteristic (ROC) curve is considered to measure the classifier's ability to discriminate between AD and HC subjects. The ROC is a graph of true positive rate (TPR) as function of false positive rate (FPR) at various cut-off values [49]. While other classifiers can be used, we employed a random forest (RF) model with 100 trees, since it is one of the most effective and general-purpose classification algorithms, and can run efficiently on large databases with thousands of input variable [50]. RF models use bootstrap aggregation to reduce model variance and, thus, chances of overfitting the training data. In addition, RFs can be used to inspect features having the most importance in the classification process [51]. We applied a 5-fold cross-validation strategy to obtain unbiased estimates of performance. In this strategy, training examples are divided into 5 equal-sized subsets and, in each fold, a subset is put aside for testing and the remaining 4 subsets are used to train the RF classifier. The final classification accuracy is computed as the average AUC obtained across the 5 folds.

To analyze the importance of individual features, we measured the increase in prediction error resulting from permuting their values across out-of-bag observations. This measure of importance is computed for every RF tree and averaged over the entire ensemble. Measured values are then normalized by dividing them by the ensemble's standard deviation, and then averaged across all 5 folds. Positive importance values indicate that a feature is predictive, whereas negative values correspond to non-predictive features.

III. EXPERIMENTAL RESULTS
A. PATIENT CHARACTERISTICS

T1-weighted MRI images of 100 AD patients and 135 HC subjects were obtained from the public OASIS database. From this dataset of 235 subjects (i.e., HC / AD, N=135/100), the HC / AD gender distribution was 97 / 59 females and 38/41 males. The median [min-max] HC / AD age was 71 [33-94] / 77 [62-96] years. The median [min-max] HC / AD of the Mini-Mental State Examination (MMSE) score was 29 [25-30] / 26 [14-30]. We found that the age, gender and MMSE score were significantly different (p < 0.01) between AD and HC subjects. Detailed demographic characteristics of the patients are presented in Table 1.
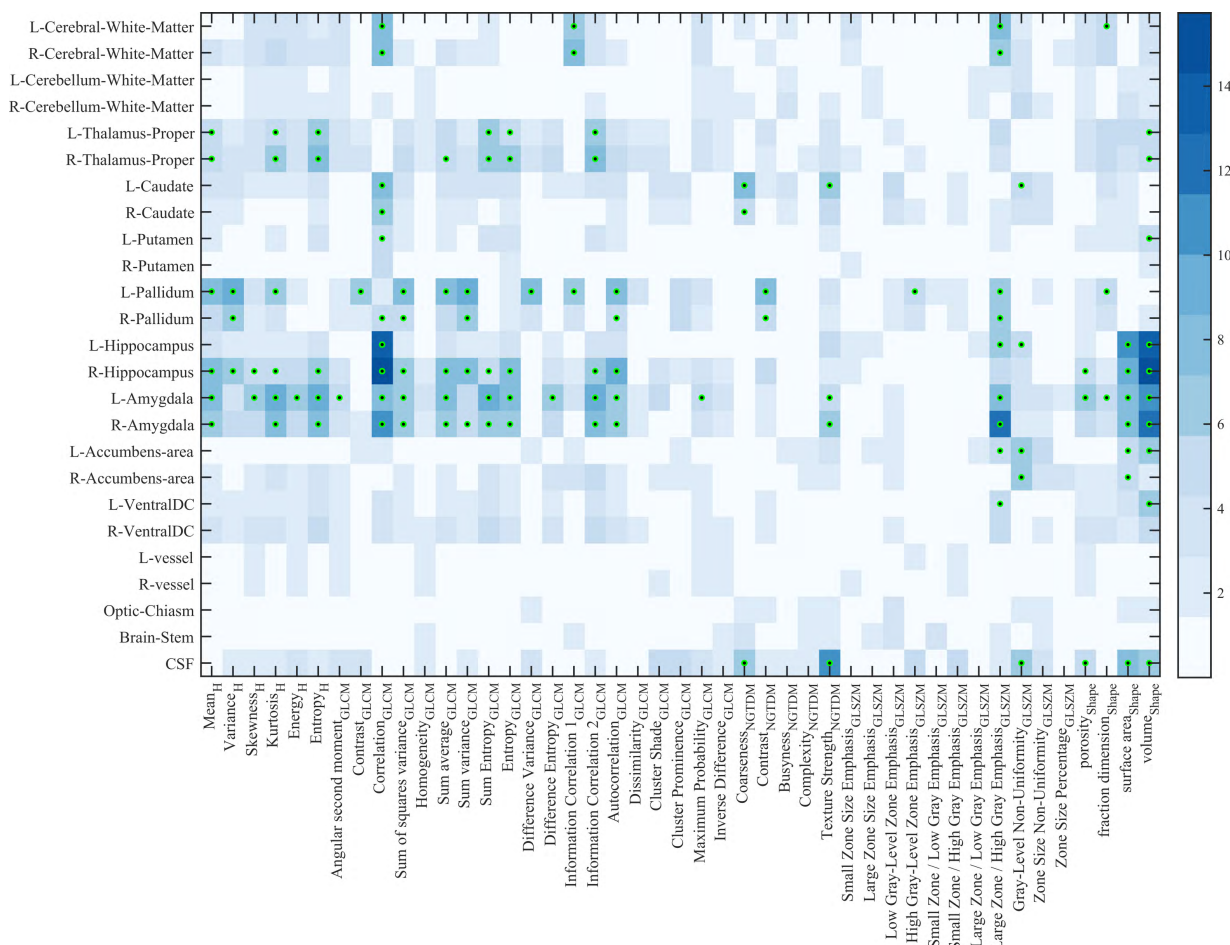
FIGURE 3. Heatmap of p values (−log10 space) obtained from Wilcoxon test for radiomic features differences between AD (n=100) and HC (n=135) subjects. Black-green circles indicate subcortical brain regions showing significant radiomic feature with corrected p < 0.01 following Holm-Bonferroni.

B. RADIOMIC FEATURES RELATED TO AD

We first investigated radiomic feature differences between AD and HC patients. Figure 3 shows the heatmap of uncorrected p values (in -log10 space) obtained from the Wilcoxon test. Significant region-feature combinations (with corrected p < 0.01) are marked with a black-green circle. Several regions show significant feature differences: cerebral-white-matter, thalamus, caudate, putamen, pallidum, hippocampus, amygdala, accumbens, ventral DC and CSF. We also observe a pronounced bilateral symmetry for the cerebral-white-matter, thalamus, caudate, pallidum, hippocampus, amygdala and accumbens regions, as well as a notable asymmetry for putamen and ventral DC regions. Moreover, we find the highest significance for GLCM-correlation, surface-area and volume features of hippocampal regions, followed by amygdala regions.

C. CLASSIFICATION USING REGION-SPECIFIC FEATURES

We assessed the usefulness of each subcortical brain region to discriminate between AD and HC subjects with the RF classifier. Using all radiomic features (n=45), the
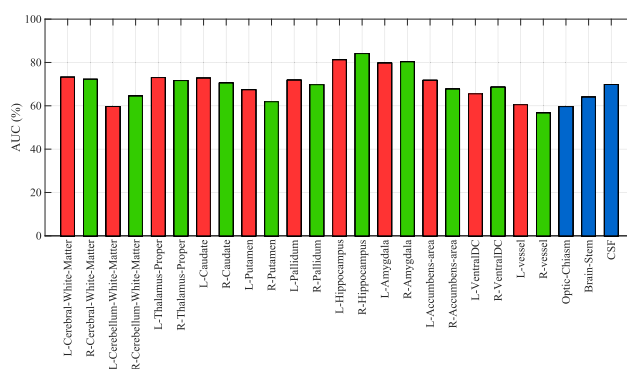

FIGURE 4. Bar graph of AUC values for classifying AD vs HC subjects using radiomic features extracted from each subcortical brain region.

resulting AUC-ROC values varied between 56.63% and 84.09%, depending on the region (Figure 4). We observe that the hippocampus achieves the highest accuracy (left: 81.19%, right: 84.09%), followed by the amygdala (left: 79.70%, right: 80.27%).
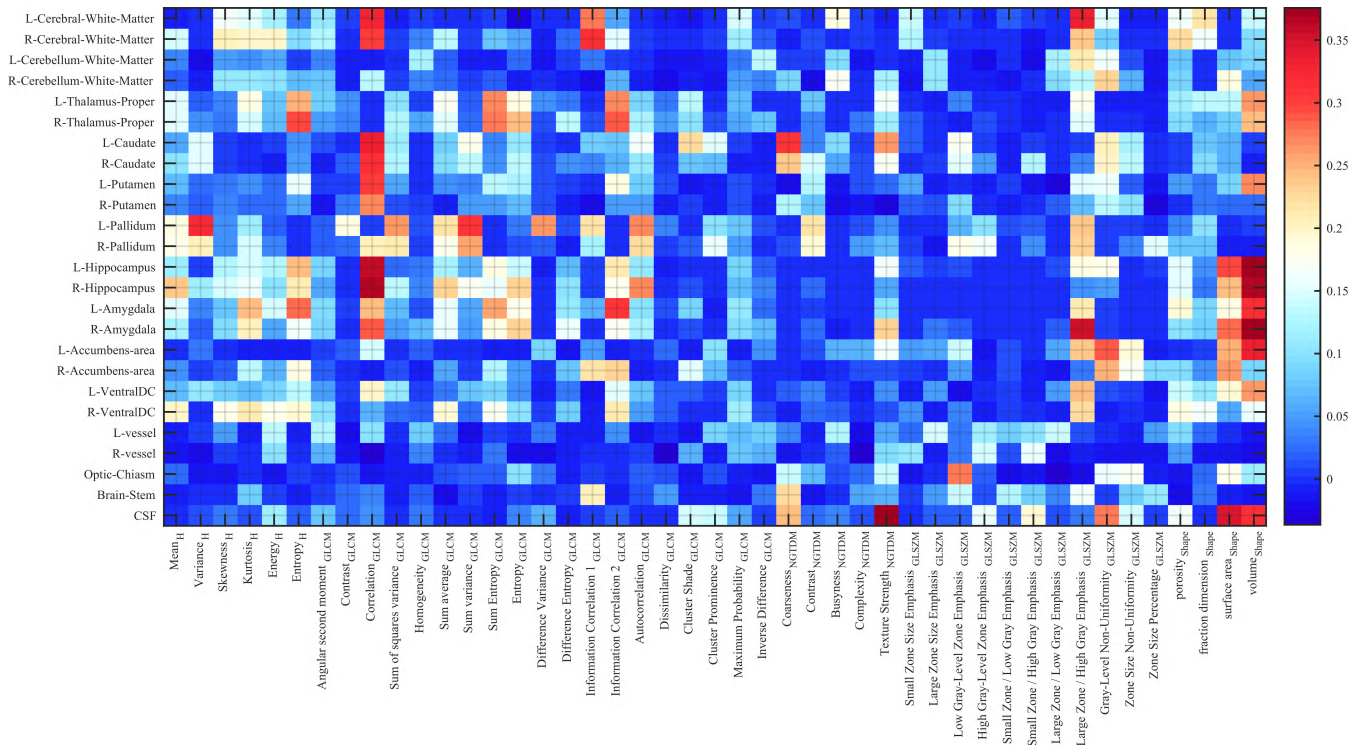
FIGURE 5. Heatmap of feature importance for classifying AD and HC subjects based on each subcortical brain region. Reported values correspond to the mean increase in prediction error obtained by permuting the values of individual features across out-of-bag observations [51].

D. IDENTIFICATION OF IMPORTANT FEATURES

Figure 5 shows the heatmap of feature importance in each of subcortical brain region. We see important features for all categories: (histogram-based) variance and entropy; (GLCM) correlation, sum-variance and information correlation; (NGTDM) coarseness and texture strength; (GLSZM) large zone/ high gray emphasis and gray-level non-uniformity; (Shape) surface area and volume. Among them, "correlation" and "volume" features in hippocampus and amygdala regions are the most dominant. This result is consistent with our previous findings which identified these regions using the Wilcoxon test and RF classifier.

E. CLASSIFICATION WITH ENTIRE FEATURE SETS

We compared the classification performance of the RF classifier trained with the 45 standard radiomic features or with the 21 proposed entropy features (i.e., entropy from 3D CNN layers). As baseline, we considered the 128 outputs of the CNN's fully-connected layer as feature vector. Note that the final CNN prediction is a linear function of these features, thus they encode information that is highly-relevant for classification.

For this analysis, we split the data of our study in two separate sets. The first set consists of 198 (AD=100, HC=98) MRI scans from demographically matched subjects with age $\geq$ 60 years. This set is used to train and test the RF classifier with different inputs (standard radiomic features, CNN entropy, or CNN fully-connected outputs), following

the 5-fold cross-validation strategy described in the previous section. The second set, which contains the remaining 37 scans, is employed to train the CNN classifier for feature extraction. Note that this two-set strategy is considered to ensure that the feature extraction is completely independent from the AD vs. HC prediction. Figure 6 shows the AUC-ROC curves obtained by the RF model for the different input features.

We see that using entropy features derived from CNN layers leads to the highest average AUC value of 92.58%, representing accuracy improvements of 8.13% and 10.90%, respectively, over standard radiomic features and CNN fully-connected outputs. This finding indicates the ability of CNN entropy to encode morphological abnormalities related to AD.

IV. DISCUSSION

Most existing models for classifying AD and HC subjects use clinical (i.e., CDR and MMSE score) or imaging volume features [52], [53]. Nomograms based on gene expression signatures, clinical features and pathological features are not yet ready to be used in daily practice. Radiomic features, which include histogram, texture, and shape features extracted from MR scans, provide a non-invasive means to predict AD [52], [54]–[60].

In this study, we showed the usefulness of radiomic features from subcortical brain regions for discriminating between AD and HC subjects. The first analysis, based on
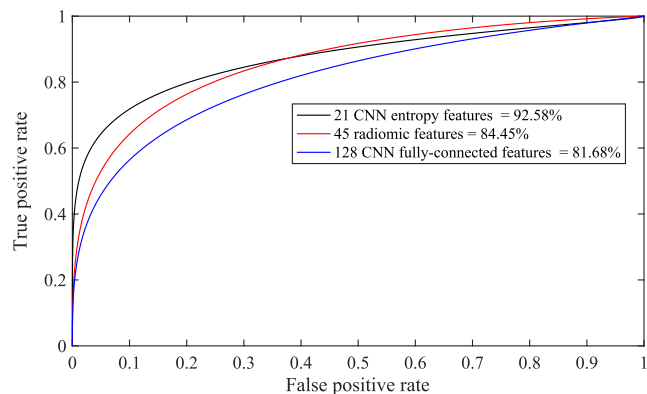
FIGURE 6. Average Area under the ROC curves for AD vs. HC prediction using the random forest (RF) classifier model with 21 entropy features derived from CNN layers (black curve), with 45 radiomic features (red curve) and with 128 features derived from CNN fully connected layer (blue curve).

the Wilcoxon test, showed the "correlation" and "volume" features from hippocampus and amygdala regions to have greatest differences between AD and HC subjects (Figure 3).

Other subcortical regions, including the cerebral white matter, thalamus, caudate, pallidum and CSF, also exhibited features which were significantly different between AD and HC subjects (corrected p < 0.01). Using random forest models to separate AD from HC subjects, we also found that the hippocampus and amygdala are the most discriminative subcortical brain regions (Fig. 4 and Fig. 5). Comparing the RF classification accuracy using the proposed 21 CNN entropy features, 45 radiomic features, and 128 features derived from the CNN fully-connected layer, we demonstrated the potential of entropy features to characterize AD (Figure 6).

Our findings are consistent with previous studies in the literature, which have found various texture and shape features to be strong biomarkers of AD [31]–[33], [54], [59], [61]–[69]. However, this work provides a more comprehensive analysis of radiomic features in individual subcortical brain regions. Specifically, our results showed the usefulness of various radiomic features across different subcortical brain regions (Figure 4). The discriminative power of radiomic features from hippocampal regions, found by our analysis, is consistent with recent studies [30], [32], [67], [70]–[73]. For example, hippocampal texture was shown to be a strong biomarker for differentiating HC from AD or MCI patients [31], [33], and hippocampal volume for detecting MCI enrichment in [66]. Our identification of differences in the amygdala of AD subjects is also consistent with previous studies [74]. Interestingly, a recent study showed that polymorphism of the APOE ϵ4 gene, the major genetic risk factor for AD, was associated with decreased hippocampal and amygdala volume in subjects with AD and MCI, but was not in healthy adults of similar age [73]. It was found that early AD disrupts intrinsic connectivity of key regions in the medial temporal lobe, including the amygdala [75]. Moreover, our study further shows that features derived from

the CSF, accumbens and caudate zones are different between AD and HC subjects.

This finding could be related to the discovery that CSF levels of Aβ42 is a strong biomarker for AD patients [76]–[79], and that the volume or integrity of accumbens, caudate, thalamus, putamen and pallidum regions [78], as well as cerebral white matter [80]–[82], was affected by AD.

In comparison to previous studies, our analysis investigated the link between AD and radiomic features in individual subcortical brain regions. This is motivated by the hypothesis that distinct regions are affected differently by AD, and that changes in separate regions can be captured by different features. This hypothesis is confirmed by the results of our experiments. In addition, we demonstrated that entropy features derived from CNN layers can improve the AUC value by about 10% compared to standard radiomic features or the full representation learned by the CNN (i.e., output of the fully-connected layer).

The current study has limitations worth mentioning. Although we used (n=235) cases from OASIS database, employing a larger independent dataset (Alzheimer disease neuroimaging initiative: ADNI) would further validate our purposed method. Moreover, considering other modalities such as FLAIR MRI and PET could increase performances. Finally, investigating additional ways to encode texture in convolution neural networks could potentially lead to better classification rates.

V. CONCLUSION

This paper proposed to investigate radiomic features derived from individual subcortical brain regions to identify AD. Our results indicate that the hippocampus and amygdala are brain regions showing the greatest differences between AD and HC subjects, and that the "correlation" and "volume" features are the most important for diagnosing AD. Furthermore, our findings suggest that entropy features derived from CNN layers could be used as an effective biomarker for AD.

REFERENCES

[1] J. R. Petrella, R. E. Coleman, and P. M. Doraiswamy, "Neuroimaging and early diagnosis of Alzheimer disease: A look to the future," *Radiology*, vol. 226, no. 2, pp. 315–336, Feb. 2003.

[2] Alzheimer's Association, "2014 Alzheimer's disease facts and figures," *Alzheimer's Dementia*, vol. 10, no. 2, pp. e47–e92, Mar. 2014.

[3] A. Wimo, G. Ljunggren, and B. Winblad, "Costs of dementia and dementia care: A review," *Int. J. Geriatric Psychiatry*, vol. 12, no. 8, pp. 841–856, Aug. 1997.

[4] R. Brookmeyer, E. Johnson, K. Ziegler-Graham, and H. M. Arrighi, "Forecasting the global burden of Alzheimer's disease," *Alzheimer's Dementia*, vol. 3, no. 3, pp. 186–191, Jul. 2007.

[5] M. W. Weiner *et al.*, "The Alzheimer's disease neuroimaging initiative: A review of papers published since its inception," *Alzheimer's Dementia*, vol. 8, no. 1, pp. S1–S68, Feb. 2012.

[6] A. Chaddad, C. Desrosiers, and M. Toews, "Multi-scale radiomic analysis of sub-cortical regions in MRI related to autism, gender and age," *Sci. Rep.*, vol. 7, Mar. 2017, Art. no. 45639.

[7] O. Kohannim *et al.*, "Boosting power for clinical trials using classifiers based on multiple biomarkers," *Neurobiol. Aging*, vol. 31, no. 8, pp. 1429–1442, Aug. 2010.

[8] Y. Fan *et al.*, "Multivariate examination of brain abnormality using both structural and functional MRI," *NeuroImage*, vol. 36, no. 4, pp. 1189–1199, Jul. 2007.

[9] P. Vemuri *et al.*, "MRI and CSF biomarkers in normal, MCI, and AD subjects diagnostic discrimination and cognitive correlations," *Neurology*, vol. 73, no. 4, pp. 287–293, Jul. 2009.

[10] C. Hinrichs, V. Singh, G. Xu, S. C. Johnson, and The Alzheimers Disease Neuroimaging Initiative, "Predictive markers for AD in a multi-modality framework: An analysis of MCI progression in the ADNI population," *NeuroImage*, vol. 55, no. 2, pp. 574–589, 2011.

[11] R. Wolz *et al.*, "Multi-method analysis of MRI images in early diagnostics of Alzheimer's disease," *PLoS ONE*, vol. 6, no. 10, p. e25446, Oct. 2011.

[12] D. Zhang, Y. Wang, L. Zhou, H. Yuan, and D. Shen, "Multimodal classification of Alzheimer's disease and mild cognitive impairment," *NeuroImage*, vol. 55, no. 3, pp. 856–867, 2011.

[13] R. S. Desikan *et al.*, "Automated MRI measures identify individuals with mild cognitive impairment and Alzheimer's disease," *Brain*, vol. 132, no. 8, pp. 2048–2057, Aug. 2009.

[14] N. Villain *et al.*, "Relationships between hippocampal atrophy, white matter disruption, and gray matter hypometabolism in Alzheimer's disease," *J. Neurosci.*, vol. 28, no. 24, pp. 6174–6181, Jun. 2008.

[15] A. Qiu, C. Fennema-Notestine, A. M. Dale, M. I. Miller, and Alzheimer's Disease Neuroimaging Initiative, "Regional shape abnormalities in mild cognitive impairment and Alzheimer's disease," *NeuroImage*, vol. 45, no. 3, pp. 656–661, Apr. 2009.

[16] M. Toews, W. Wells, III, D. L. Collins, and T. Arbel, "Feature-based morphometry: Discovering group-related anatomical patterns," *NeuroImage*, vol. 49, no. 3, pp. 2318–2327, 2010.

[17] M. Li *et al.*, "An efficient approach for differentiating Alzheimer's disease from normal elderly based on multicenter MRI using gray-level invariant features," *PLoS ONE*, vol. 9, no. 8, p. e105563, 2014.

[18] M. Yoshita *et al.*, "Extent and distribution of white matter hyperintensities in normal aging, MCI, and AD," *Neurology*, vol. 67, no. 12, pp. 2192–2198, Dec. 2006.

[19] R. Barber *et al.*, "White matter lesions on magnetic resonance imaging in dementia with Lewy bodies, Alzheimer's disease, vascular dementia, and normal aging," *J. Neurol., Neurosurg. Psychiatry*, vol. 67, no. 1, pp. 66–72, 1999.

[20] F.-E. de Leeuw *et al.*, "Prevalence of cerebral white matter lesions in elderly people: A population based magnetic resonance imaging study. The Rotterdam Scan Study," *J. Neurol. Neurosurg. Psychiatry*, vol. 70, no. 1, pp. 9–14, Jan. 2001.

[21] A. M. Tuladhar *et al.*, "Relationship between white matter hyperintensities, cortical thickness, and cognition," *Stroke*, vol. 46, no. 2, pp. 425–432, Feb. 2015.

[22] M. Fujishima, N. Maikusa, K. Nakamura, M. Nakatsuka, H. Matsuda, and K. Meguro, "Mild cognitive impairment, poor episodic memory, and late-life depression are associated with cerebral cortical thinning and increased white matter hyperintensities," *Frontiers Aging Neurosci.*, vol. 6, p. 306, Nov. 2014.

[23] V. Kumar *et al.*, "Radiomics: The process and the challenges," *Magn. Reson. Imag.*, vol. 30, no. 9, pp. 1234–1248, Nov. 2012.

[24] R. Lambin *et al.*, "Radiomics: Extracting more information from medical images using advanced feature analysis," *Eur. J. Cancer*, vol. 48, no. 4, pp. 441–446, 2012.

[25] P. Mondal, J. Mukhopadhyay, S. Sural, and P. P. Bhattacharyya, "3D-SIFT feature based brain atlas generation: An application to early diagnosis of Alzheimer's disease," in *Proc. Int. Conf. Med. Imag., m-Health Emerg. Commun. Syst. (MedCom)*, Nov. 2014, pp. 342–347.

[26] X. He, L. Chen, X. Li, and H. Fu, "Brain image feature recognition method for Alzheimer's disease," *Cluster Comput.*, pp. 1–9, Feb. 2018.

[27] A. Ayaz, M. Z. Ahmad, K. Khurshid, and A. M. Kamboh, "MRI based automated diagnosis of Alzheimer's: Fusing 3D wavelet-features with clinical data," in *Proc. 39th Annu. Int. Conf. IEEE Eng. Med. Biol. Soc. (EMBC)*, Jul. 2017, pp. 1210–1213.

[28] N. Kodama, Y. Kawase, and K. Okamoto, "Application of texture analysis to differentiation of dementia with lewy bodies from Alzheimer's disease on magnetic resonance images," in *Proc. World Congr. Med. Phys. Biomed. Eng.* Berlin, Germany: Springer, 2007, pp. 1444–1446.

[29] J. Zhang, C. Yu, G. Jiang, W. Liu, and L. Tong, "3D texture analysis on MRI images of Alzheimer's disease," *Brain Imag. Behav.*, vol. 6, no. 1, pp. 61–69, Mar. 2012.

[30] L. Sørensen *et al.*, "Early detection of Alzheimer's disease using MRI hippocampal texture," *Hum. Brain Mapping*, vol. 37, no. 3, pp. 1148–1161, 2016.

[31] J. Liu, J. Wang, B. Hu, F.-X. Wu, and Y. Pan, "Alzheimer's disease classification based on individual hierarchical networks constructed with 3-D texture features," *IEEE Trans. Nanobiosci.*, vol. 16, no. 6, pp. 428–437, Sep. 2017.

[32] L. Sørensen *et al.*, "Differential diagnosis of mild cognitive impairment and Alzheimer's disease using structural MRI cortical thickness, hippocampal shape, hippocampal texture, and volumetry," *NeuroImage, Clin.*, vol. 13, pp. 470–482, 2017.

[33] C. V. Dolph, M. Alam, Z. Shboul, M. D. Samad, and K. M. Iftekharuddin, "Deep learning of texture and structural features for multiclass Alzheimer's disease classification," in *Proc. Int. Joint Conf. Neural Netw. (IJCNN)*, May 2017, pp. 2259–2266.

[34] B. Fischl, "Freesurfer," *NeuroImage*, vol. 62, no. 2, pp. 774–781, Aug. 2012.

[35] A. Chaddad, B. Naisiri, M. Pedersoli, E. Granger, C. Desrosiers, and M. Toews. (Nov. 2017). "Modeling information flow through deep neural networks." [Online]. Available: https://arxiv.org/abs/1712.00003

[36] D. S. Marcus, T. H. Wang, J. Parker, J. G. Csernansky, J. C. Morris, and R. L. Buckner, "Open access series of imaging studies (OASIS): Cross-sectional MRI data in young, middle aged, nondemented, and demented older adults," *J. Cogn. Neurosci.*, vol. 19, no. 9, pp. 1498–1507, Sep. 2007.

[37] F. Tsai, C.-K. Chang, J.-Y. Rau, T.-H. Lin, and G.-R. Liu, "3D computation of gray level co-occurrence in hyperspectral image cubes," *Lect. Notes Comput. Sci.*, vol. 4679, pp. 429–440, 2007.

[38] R. M. Haralick, "Statistical and structural approaches to texture," *Proc. IEEE*, vol. 67, no. 5, pp. 786–804, May 1979.

[39] M. Amadasun and R. King, "Textural features corresponding to textural properties," *IEEE Trans. Syst., Man, Cybern.*, vol. 19, no. 5, pp. 1264–1274, Sep. 1989.

[40] G. Thibault *et al.*, "Texture indexes and gray level size zone matrix. Application to cell nuclei classification," in *Proc. 10th Int. Conf. Pattern Recognit. Inf. Process.*, 2009, pp. 140–145.

[41] Z. Lewandowski and H. Beyenal, *Fundamentals of Biofilm Research*. Boca Raton, FL, USA: CRC Press, 2007.

[42] N. Schuff *et al.*, "MRI of hippocampal volume loss in early Alzheimer's disease in relation to ApoE genotype and biomarkers," *Brain*, vol. 132, no. 4, pp. 1067–1077, Apr. 2009.

[43] D. Shen, G. Wu, and H. Suk, "Deep learning in medical image analysis," *Annu. Rev. Biomed. Eng.*, vol. 19, pp. 221–248, Jun. 2017.

[44] G.-W. Yang and H.-F. Jing, "Multiple convolutional neural network for feature extraction," in *Proc. Int. Conf. Intell. Comput.* Fuzhou, China: Springer, Aug. 2015, pp. 104–114.

[45] B. Wu *et al.*, "FF-CNN: An efficient deep neural network for mitosis detection in breast cancer histological images," in *Proc. 21st Annu. Conf. MIUA*, Edinburgh, U.K., Jul. 2017, pp. 249–260.

[46] Y. Xu *et al.*, "Large scale tissue histopathology image classification, segmentation, and visualization via deep convolutional activation features," *Bioinformatics*, vol. 18, no. 1, p. 281, Dec. 2017.

[47] R. Shwartz-Ziv and N. Tishby. (Mar. 2017). "Opening the black box of deep neural networks via information." [Online]. Available: https://arxiv.org/abs/1703.00810

[48] S. Holm, "A simple sequentially rejective multiple test procedure," *Scand. J. Statist.*, vol. 6, no. 2, pp. 65–70, 1979.

[49] A. P. Bradley, "ROC curve equivalence using the Kolmogorov–Smirnov test," *Pattern Recognit. Lett.*, vol. 34, no. 5, pp. 470–475, 2013.

[50] L. Breiman, "Random forests," *Mach. Learn.*, vol. 45, no. 1, pp. 5–32, 2001.

[51] K. J. Archer and R. V. Kimes, "Empirical characterization of random forest variable importance measures," *Comput. Statist. Data Anal.*, vol. 52, no. 4, pp. 2249–2260, Jan. 2008.

[52] M.-J. Chiu *et al.*, "Plasma tau as a window to the brain—Negative associations with brain volume and memory function in mild cognitive impairment and early alzheimer's disease," *Hum. Brain Mapping*, vol. 35, no. 7, pp. 3132–3142, 2014.

[53] Y.-B. Hu *et al.*, "Diagnostic value of microRNA for Alzheimer's disease: A systematic review and meta-analysis," *Front Aging Neurosci.*, vol. 8, p. 13, Feb. 2016.

[54] M. S. de Oliveira *et al.*, "MR imaging texture analysis of the corpus callosum and thalamus in amnestic mild cognitive impairment and mild Alzheimer disease," *Amer. J. Neuroradiol.*, vol. 32, no. 1, pp. 60–66, Jan. 2011.

[55] J. Shin, S.-Y. Lee, S. J. Kim, S.-H. Kim, S.-J. Cho, and Y.-B. Kim, "Voxel-based analysis of Alzheimer's disease PET imaging using a triplet of radiotracers: PIB, FDDNP, and FDG," *NeuroImage*, vol. 52, no. 2, pp. 488–496, Aug. 2010.

[56] P. A. Thomann, T. Wüstenberg, J. Pantel, M. Essig, and J. Schröder, "Structural changes of the corpus callosum in mild cognitive impairment and Alzheimer's disease," *Dementia Geriatric Cognit. Disorders*, vol. 21, no. 4, pp. 215–220, 2006.

[57] T. M. Chaim, F. L. Duran, R. R. Uchida, C. A. M. Périco, C. C. de Castro, and G. F. Busatto, "Volumetric reduction of the corpus callosum in Alzheimer's disease *in vivo* as assessed with voxel-based morphometry," *Psychiatry Res., Neuroimaging*, vol. 154, no. 1, pp. 59–68, 2007.

[58] S. E. Rose, L. Andrew, and J. B. Chalk, "Gray and white matter changes in Alzheimer's disease: A diffusion tensor imaging study," *J. Magn. Reson. Imag.*, vol. 27, no. 1, pp. 20–26, 2008.

[59] M. M. Abdelsamea. (Dec. 2014). "An automatic seeded region growing for 2D biomedical image segmentation." [Online]. Available: https://arxiv.org/abs/1412.3958

[60] A. Chaddad, C. Desrosiers, and M. Toews, "Local discriminative characterization of MRI for Alzheimer's disease," in *Proc. 13th IEEE Int. Symp. Biomed. Imag., (ISBI)*, Prague, Czech Republic, Apr. 2016, pp. 1–5.

[61] R. Maani, Y. H. Yang, and S. Kalra, "Voxel-based texture analysis of the brain," *PLoS ONE*, vol. 10, no. 3, p. e0117759, Mar. 2015.

[62] F. de Vos *et al.*, "Combining multiple anatomical MRI measures improves Alzheimer's disease classification," *Hum. Brain Mapping*, vol. 37, no. 5, pp. 1920–1929, 2016.

[63] H. Liu, X. Zhou, H. Jiang, H. He, X. Liu, and Alzheimer's Disease Neuroimaging Initiative, "A semi-mechanism approach based on MRI and proteomics for prediction of conversion from mild cognitive impairment to Alzheimer's disease," *Sci. Rep.*, vol. 6, Jun. 2016, Art. no. 26712.

[64] B. Cheng *et al.*, "Multimodal manifold-regularized transfer learning for MCI conversion prediction," *Brain Imag. Behav.*, vol. 9, no. 4, pp. 913–926, 2015.

[65] F. J. Martinez-Murcia *et al.*, "Evaluating Alzheimer's disease diagnosis using texture analysis," in *Proc. Med. Image Understand. Anal.*, Edinburgh, U.K., Jul. 2017, pp. 470–481.

[66] L. Sørensen, C. Igel, and M. Nielsen, "MCI trial enrichment using MRI hippocampus texture," *Alzheimer's Dementia, J. Alzheimer's Assoc.*, vol. 12, no. 7, pp. P108–P109, 2016.

[67] P. Keserwani, V. S. C. Pammi, O. Prakash, A. Khare, and M. Jeon, "Classification of Alzheimer disease using Gabor texture feature of hippocampus region," *Int. J. Image, Graph. Signal Process.*, vol. 8, no. 6, p. 13, 2016.

[68] E.-J. Hwang *et al.*, "Texture analyses of quantitative susceptibility maps to differentiate Alzheimer's disease from cognitive normal and mild cognitive impairment," *Med. Phys.*, vol. 43, no. 8, pp. 4718–4728, 2016.

[69] K. Oppedal, K. Engan, T. Eftestøl, M. Beyer, and D. Aarsland, "Classifying Alzheimer's disease, Lewy body dementia, and normal controls using 3D texture analysis in magnetic resonance images," *Biomed. Signal Process. Control*, vol. 33, pp. 19–29, Mar. 2017.

[70] K. Zhao *et al.*, "Early classification of Alzheimer's disease using hippocampal texture from structural MRI," *Proc. SPIE, Med. Imag., Biomed. Appl. Mol., Struct., Funct. Imag.*, vol. 10137, p. 101372E, Mar. 2017, doi: 10.1117/12.2254198.

[71] D. Sarwinda and A. Bustamam, "Detection of Alzheimer's disease using advanced local binary pattern from hippocampus and whole brain of MR images," in *Proc. Int. Joint Conf. Neural Netw. (IJCNN)*, Jul. 2016, pp. 5051–5056.

[72] C. Schroeder *et al.*, "Hippocampal shape alterations are associated with regional Aβ load in cognitively normal elderly individuals," *Eur. J. Neurosci.*, vol. 45, no. 10, pp. 1241–1251, May 2017.

[73] M. K. Lupton *et al.*, "The effect of increased genetic risk for Alzheimer's disease on hippocampal and amygdala volume," *Neurobiol. Aging*, vol. 40, pp. 68–77, Apr. 2016.

[74] J. Yang *et al.*, "Voxelwise meta-analysis of gray matter anomalies in Alzheimer's disease and mild cognitive impairment using anatomic likelihood estimation," *J. Neurol. Sci.*, vol. 316, nos. 1–2, pp. 21–29, May 2012.

[75] M. Ortner *et al.*, "Progressively disrupted intrinsic functional connectivity of basolateral amygdala in very early Alzheimer's disease," *Front Neurol.*, vol. 7, p. 132, Sep. 2016.

[76] R. J. Bateman *et al.*, "Clinical and biomarker changes in dominantly inherited Alzheimer's disease," *New England J. Med.*, vol. 367, no. 9, pp. 795–804, 2012.

[77] K. Blennow, H. Hampel, M. Weiner, and H. Zetterberg, "Cerebrospinal fluid and plasma biomarkers in Alzheimer disease," *Nature Rev. Neurol.*, vol. 6, no. 3, pp. 131–144, 2010.

[78] C. Möller *et al.*, "More atrophy of deep gray matter structures in frontotemporal dementia compared to Alzheimer's disease," *J. Alzheimer's Disease*, vol. 44, no. 2, pp. 635–647, 2015.

[79] J. B. Pereira, E. Westman, O. Hansson, and Alzheimer's Disease Neuroimaging Initiative, "Association between cerebrospinal fluid and plasma neurodegeneration biomarkers with brain atrophy in Alzheimer's disease," *Neurobiol. Aging*, vol. 58, pp. 14–29, Oct. 2017.

[80] J. C. de Groot, F.-E. de Leeuw, M. Oudkerk, A. Hofman, J. Jolles, and M. M. B. Breteler, "Cerebral white matter lesions and subjective cognitive dysfunction The Rotterdam Scan Study," *Neurology*, vol. 56, no. 11, pp. 1539–1545, Jun. 2001.

[81] G. T. Whitman, T. Tang, A. Lin, and R. W. Baloh, "A prospective study of cerebral white matter abnormalities in older people with gait dysfunction," *Neurology*, vol. 57, no. 6, pp. 990–994, Sep. 2001.

[82] J. C. de Groot *et al.*, "Cerebral white matter lesions and cognitive function: The Rotterdam Scan Study," *Ann. Neurol.*, vol. 47, no. 2, pp. 145–151, Feb. 2000.

AHMAD CHADDAD received the Ph.D. degree in systems engineering from the University of Lorraine in 2012. He was a Post-Doctoral Research Fellow with the University of Texas MD Anderson Cancer Center from 2013 to 2015 and with McGill University from 2016 to 2017. He joined the Department of Automated Manufacturing Engineering, ETS, University of Quebec, as an Adjunct Professor. He is a member of the Laboratory of Design, Optimization and Modelling of Systems.

His current research interests include biomedical imaging, signal and image processing, pattern recognition, and microelectronics circuits.

CHRISTIAN DESROSIERS received the Ph.D. degree in computer engineering from Polytechnique Montreal in 2008. He was a Post-Doctoral Researcher with the University of Minnesota, where he focused on the topic of machine learning. In 2009, he joined the Department of Software and IT Engineering, ETS, University of Quebec, as a Professor. He is the Co-Director of the Laboratoire d'imagerie, de vision et d'intelligence artificielle and a member of the REPARTI Research Network.

His main research interests focus on machine learning, image processing, computer vision, and medical imaging.

TAMIM NIAZI received the Doctor of Medicine and Master of Surgery degree from McGill University in 2001. He continued his internship and residency with the McGill University Health Centre. During 2006–2007, he was the Clinical Trials Fellow with the National Cancer Institute of Canada Clinical Trials Group. He is currently a Professor Adjoint with the Department of Oncology, McGill University, where he is also the Fellowship Co-Director with the Division of Radiation Oncology.

He has presented and published over 50 peer-reviewed academic works.

• • •